



OPEN Research on the impact of land use and land cover changes on local meteorological conditions and surface ozone in the north China plain from 2001 to 2020

Chunsheng Fang^{1,2,3}, Xinlong Li^{1,2}, Juan Li^{1,2}, Jiaqi Tian^{1,2} & Ju Wang^{1,2,3}✉

Land use and land cover changes (LULCC) alter local surface attributes, thereby modifying energy balance and material exchanges, ultimately impacting meteorological parameters and air quality. The North China Plain (NCP) has undergone rapid urbanization in recent decades, leading to dramatic changes in land use and land cover. This study utilizes the 2020 land use and land cover data obtained from the MODIS satellite to replace the default 2001 data in the Weather Research and Forecasting-Community Multiscale Air Quality (WRF-CMAQ) model. It simulates and analyzes the direct impact of LULCC on meteorological parameters and the indirect impact on surface ozone (O₃) concentration through physical and chemical processes in the North China Plain during July in the summer. Six rapidly urbanizing cities were selected to represent the North China Plain. The results show that LULCC significantly increased sensible heat flux and 2-m temperature in rapidly urbanizing areas throughout the diurnal cycle, with more pronounced effects during the daytime, ranging from 6.49 to 23.46 W/m² and 0.20–0.59 °C, respectively. The 10-m wind speed decreased at night and increased during the day, with changes ranging from –0.43 to 0.27 m/s at night and –0.16 to 0.15 m/s during the day. The planetary boundary layer height generally increased, with a larger rise during the daytime, ranging from 23.63 to 84.74 m. Simultaneously, surface O₃ concentrations increased during both daytime and nighttime. The daytime increase ranged from 2.89 to 9.82 µg/m³, while the nighttime increase ranged from 1.76 to 7.77 µg/m³. LULCC enhanced meteorological and chemical processes as well as vertical transport, leading to an increase in O₃. At the same time, it reduced the increase in O₃ through horizontal transport and dry deposition processes. These changes are related to the meteorological variations. The impact on O₃ concentrations was not limited to the surface but extended to the top of the planetary boundary layer (approximately 1500 m). Below 500 m, vertical transport increased O₃ concentrations, while horizontal transport decreased O₃ concentrations. Additionally, the meteorological and chemical processes induced by LULCC showed enhanced effects above the surface, whereas the dry deposition process had a smaller impact on O₃ concentrations above the surface. This study reveals the significant impact of urban expansion on regional meteorological parameters and air quality. It optimizes the model's simulation of regional air quality and provides new insights into understanding the effects of urbanization on meteorological conditions and air quality.

Keywords Land use, Land cover, North China plain, Urban meteorology, Air quality

In the past decade, with the continuous acceleration of industrialization and urbanization processes, air quality in China has deteriorated gradually. In response, China introduced the “Air Pollution Prevention and Control Action Plan” in 2013. Since then, air quality in China has gradually improved, with a steady decline in fine particulate matter (PM_{2.5})^{1,2}. However, during this period, the problem of ozone (O₃) pollution has become more severe^{3,4}. Since 2013, surface O₃ has become one of the main environmental issues in the North China

¹College of New Energy and Environment, Jilin University, Changchun 130012, China. ²Key Laboratory of Groundwater Resources and Environment, Ministry of Education, Jilin University, Changchun 130021, China. ³Jilin Province Key Laboratory of Water Resources and Environment, Jilin University, Changchun 130021, China. ✉email: wangju@jlu.edu.cn

Plain^{5,6}. Severe O₃ pollution not only poses risks to human health and ecosystems but also affects socio-economic aspects^{7,8}. Multiple studies have demonstrated that the formation of O₃ is closely related to human activities and is also influenced by meteorological parameters, land cover types, and other factors^{9–11}.

O₃ can be formed through nonlinear reactions involving precursor substances such as nitrogen oxides (NO_x) and volatile organic compounds (VOCs), or it can accumulate through regional transport processes^{12,13}. Therefore, meteorological parameters (such as temperature, humidity, radiation, cloud cover, and wind speed) may influence surface O₃ and its precursor concentrations by affecting photochemical reaction rates and vertical transport. The increase in O₃ levels is typically attributed to higher temperatures and solar radiation flux^{14,15}, along with lower humidity and cloud cover^{16,17}. Moreover, these meteorological parameters can indirectly influence the generation of O₃ precursors, thereby affecting the variations in O₃ concentrations¹². Additionally, wind patterns can accumulate surface O₃ by influencing its horizontal and vertical transport^{18,19}. Previous studies have highlighted the significance of meteorological parameters in influencing O₃^{5,9,20}. Therefore, investigating the impact of meteorological parameters is essential. As urban areas expand, land use and land cover changes (LULCC) can impact local meteorological parameters, air quality levels, and even regional climate conditions^{21,22}. This is typically achieved through alterations in surface roughness, albedo, and heat storage characteristics^{23,24}. The impact of LULCC varies across different regions, but rapid urbanization and decreased surface vegetation intensify its effects on regional meteorological fields and air quality²⁵. Therefore, there is a growing need to study the effects of LULCC through numerical simulation methods.

Many previous studies have utilized numerical and modeling simulation methods to establish the relationship between meteorological parameters and surface O₃ concentration, as well as the impact of LULCC on urban meteorological fields and O₃ in China^{26,27}. Yang et al.²⁸, synthesizing 212 articles utilizing air quality model (AQM) simulations of O₃, demonstrated that meteorological factors consistently contribute to the accumulation of O₃ concentrations. They recommended optimizing land use data to improve the simulation effectiveness of O₃. Qu et al.²⁹ employed the Weather Research and Forecasting (WRF) model to investigate surface temperature changes resulting from land use variations in the North China Plain from 1992 to 2005. They found that the regional average surface temperature increased by 0.03 °C per year, and the spatial distribution of climate change closely resembled the changes in land use. Jiang et al.³⁰ utilized the Weather Research and Forecasting with Chemistry (WRF-Chem) model to investigate the impacts of current and future climate change and land use type variations on O₃ concentrations in Texas. They found that the combined influence of these two factors on O₃ concentrations could reach up to 6.2 ppbv, and land use changes could lead to an increase of 2–3 days in extreme O₃ events in August. Modeling studies on the impact of rapid urbanization in the Sichuan Basin have revealed that in regions undergoing rapid urbanization, both temperature and planetary boundary layer height increase. Changes in meteorological phenomena also alter the physical and chemical processes associated with variations in PM_{2.5} and O₃ concentrations, ultimately leading to changes in pollutant concentrations^{31,32}. Research on the Yangtze River Delta and the Beijing-Tianjin-Hebei region has consistently confirmed that LULCC leads to an increase in surface temperature, a decrease in wind speed, and exacerbation of vertical transport. These factors undoubtedly contribute to the accumulation of surface O₃^{33,34}.

As China's anthropogenic emissions continue to decrease, the influence of meteorological parameters on pollutants is receiving increasing attention. Understanding the physical and chemical impact processes of meteorological parameters on surface O₃ formation is essential. The North China Plain, with its vast territory and concentration of large cities, has seen continuous expansion of urban areas since 2001, prompting greater concern about the associated atmospheric pollution issues. In this study, we utilized the Weather Research and Forecasting-Community Multiscale Air Quality (WRF-CMAQ) model to investigate the impact of land use and land cover changes on summer urban meteorology and surface O₃ in the North China Plain (NCP) since 2001. We replaced the default 2001 land use data in WRF with land use and land cover data obtained from the Moderate Resolution Imaging Spectroradiometer (MODIS). Additionally, we employed the Process Analysis (PA) module of the CMAQ model to quantitatively simulate the physical and chemical processes influencing O₃. This research aims to understand the potential impacts of land use changes and provide insights for designing pollution control measures while avoiding adverse meteorological effects.

Data and methods

Model configuration description

We used the WRF v4.3.3 (<https://www.mmm.ucar.edu/models/wrf>)³⁵ to simulate meteorological parameters. The initial and boundary conditions were obtained from the Final (FNL) analysis dataset provided by the National Centers for Environmental Prediction (NCEP)³⁶, with a temporal resolution of 6 h and a spatial resolution of 1.0° × 1.0° (<https://rda.ucar.edu/datasets/d083002/>). The model was configured with three nested domains, each with horizontal resolutions of 27, 9, and 3 km, respectively. The outermost domain covered most parts of China, the middle domain encompassed the entire NCP, and the innermost domain included six administrative regions: Beijing (BJ), Tianjin (TJ), Hebei (HB), Shanxi (SX), Henan (HN), and Shandong (SD) provinces (Fig. 1a). The model has a top at 50 hPa and is configured with 45 vertical layers, with a higher density near the surface and a lower density at higher altitudes. The CMAQv5.4 model (<https://www.epa.gov/cmaq>)³⁷ is used to simulate surface O₃ concentrations, with the necessary meteorological input data provided by WRF. The nested domain settings and horizontal resolution are the same as those of WRF, with 45 vertical layers also set for both models. The physical parameterization schemes used by the WRF and CMAQ models are shown in Tables S1 and S2. These schemes have also been used in other studies focusing on the North China Plain or China as a whole^{38–40}. Additionally, the same configuration schemes have been validated in our previous studies to be applicable across various regions in China^{41,42}. The emission inventory utilized the 2020 Multi-resolution Emission Inventory model for Climate and air pollution research (MEIC) developed by Tsinghua University (<http://meicmodel.org>

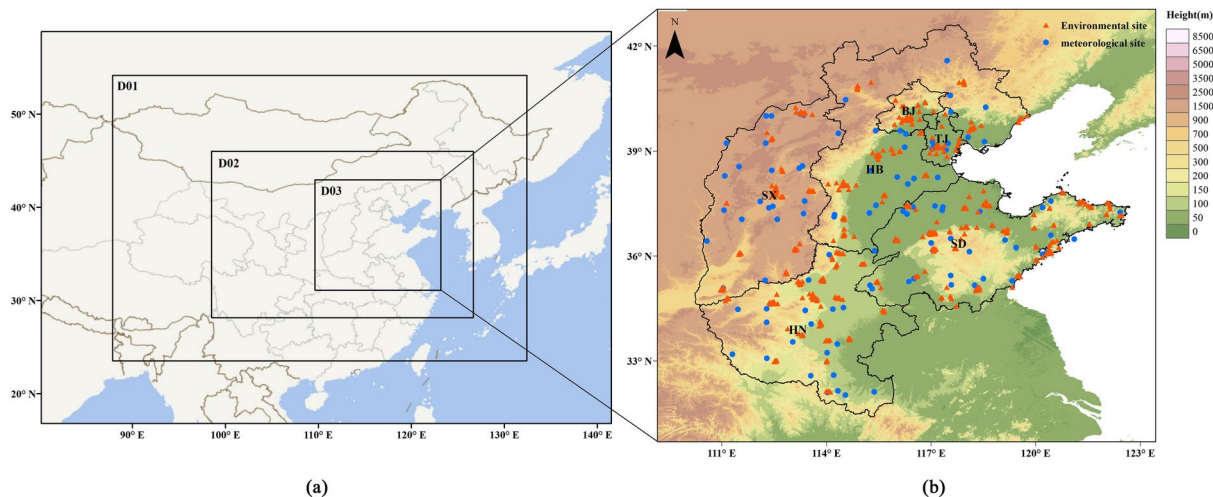


Fig. 1. Schematic diagram of the model's three nested domains (a) and the locations and elevations of all meteorological monitoring stations (blue circles) and background atmospheric pollution monitoring stations (orange triangles) within the NCP (b). Note: All the maps in this paper were created using ArcGIS v10.8⁴⁶ (<https://www.esri.com/>).

.cn^{43,44}. Biogenic emissions were calculated using the Model of Emissions of Gases and Aerosols from Nature version 2.1 (MEGAN v2.1) and meteorological inputs from the WRF model⁴⁵.

To investigate the impact of LULCC on local meteorology and pollutant concentrations, it is necessary to replace the default 2001 land cover and land use dataset in WRF with the 2020 MODIS MCD12Q1 product (<https://lpdaac.usgs.gov/products/mcd12q1v061/>)⁴⁷. The downloaded MCD12Q1 product uses the IGBP17 classification method (Table S3). In the WRF model simulation, no adjustments were made to the meteorological conditions to better isolate the individual impact of changes in land cover and land use data. By analyzing the pollutant monitoring data from six administrative regions in the North China Plain for the year 2020, it was found that ozone pollution was most severe in the months of July and August. Therefore, the study period was selected as July of the years 2001 and 2020. A spin-up period of 5 days before July (June 26–June 30) was set to avoid adverse effects from initial conditions^{48,49}.

Process analysis

The process analysis module can quantify the contribution of individual processes to model predictions and display the relative importance of each process. Additionally, the information provided by the chemical process analysis can be used to identify key features of different chemical mechanisms. The process analysis module can be divided into two parts: Integrated Process Rate (IPR) analysis and Integrated Reaction Rate (IRR) analysis. IPR concerns the net impact of all physical processes and chemical reactions on model predictions. IRR analysis details the chemical transformations described in the model's chemical mechanisms. For more details on process analysis, refer to the study by Jang et al.^{50,51}.

This study uses the IPR module in PA analysis to analyze the indirect effects of LULCC-induced physical and chemical changes on surface O_3 . O_3 concentration depends on various physical processes (such as horizontal transport⁵² and vertical mixing⁵³), photochemical processes, and deposition removal processes⁵⁴. The processes selected for this study include horizontal advection (HADV), vertical advection (ZADV), horizontal diffusion (HDIF), vertical diffusion (VDIF), gas-phase chemistry (CHEM), dry deposition (DDEP), aerosol processes (AERO), and cloud processes (CLDS). Horizontal transport is the sum of horizontal advection and horizontal diffusion, while vertical transport is the sum of vertical advection and vertical diffusion. Cloud processes involve liquid-phase reactions and cloud/rain scavenging, and aerosol processes involve condensation, atmospheric new particle formation, and aerosol growth. Therefore, in this study, the DDEP, AERO, and CLDS processes are collectively referred to as the deposition (DEPO) process, the HADV and HDIF processes are collectively referred to as the horizontal transport (HTRA) process, and the ZADV and VDIF processes are collectively referred to as the vertical transport (VTTRA) process⁵⁵.

Data sources and model evaluation

The meteorological monitoring data and pollutant monitoring data used in this study are sourced from the China Meteorological Data Service Center (<http://data.cma.cn/>) and the China National Environmental Monitoring Center (<http://www.cnemc.cn/>), respectively. All monitoring data are generated hourly. Meteorological monitoring data included temperature and wind speed, while pollutant monitoring data focused on ozone. To ensure the suitability of the data for validating model simulation results, preprocessing was conducted according to the "Technical Specifications for Ambient Air Quality Monitoring" (HJ 664-2013), which involved filtering out spatial and temporal outliers from the monitoring data. The locations of all air quality stations and meteorological stations within the NCP are depicted in Fig. 1b.

The simulation results of the WRF and CMAQ models were evaluated using Mean Bias (MB), Mean Error (ME), Root Mean Square Error (RMSE), Normalized Mean Bias (NMB), Normalized Mean Error (NME), and Pearson Correlation Coefficient (R). These evaluation metrics have also been widely used in other studies to validate the reliability of the WRF and CMAQ models^{56–58}. The calculation formulas for each metric are provided in Supplementary Material Table S4.

Scenario design

In this study, we primarily focused on the direct impact of LULCC on meteorological parameters in the NCP region and the associated physical changes that indirectly affect surface O₃. We did not consider the direct impact of LULCC on surface O₃ (such as changes in anthropogenic emission inventories). Therefore, we set up two scenarios with different land use data (Table 1). The Case 2001 scenario uses the default 2001 land use and land cover data in the WRF model to represent the land use pattern in the NCP region for 2001. The Case 2020 scenario uses the 2020 land use and land cover data to replace the default data, representing the land use pattern in the NCP region for 2020. The analysis of monitoring data revealed that O₃ pollution frequently occurs in July in the study area, thus July 2020 was selected as the study period. Additionally, biogenic emissions for both scenarios were recalculated based on the LULC year, a task completed using the MEGAN tool described in the methods section. Apart from this, the model setup, parameterization schemes, and anthropogenic emission inventories were identical for both scenarios. It is important to note that the simulation period for meteorological parameters in both scenarios was selected as July 2020. Therefore, the differences in simulation results between the two scenarios (Case 2020–Case 2001) can be used to quantify the direct impact of LULCC on meteorological parameters and the indirect impact on surface O₃.

As shown in Fig. 2a, China's urbanization rate increased from 37.66% in 2001 to 63.89% in 2020, nearly doubling (data source: National Bureau of Statistics of China: <https://data.stats.gov.cn/>). During this period, the NCP also experienced significant urban expansion. The most drastic changes were observed in major cities within each province, where rapid transformation from farmland to urban built-up areas took place. In contrast, such changes were less pronounced in rural areas and regions with sparse human activity. These transformations could alter surface characteristics, thereby affecting regional meteorological parameters and near-surface air quality. To clearly demonstrate the impact of LULCC, we selected a representative city from each of the six administrative regions in the NCP for study. In addition to the two municipalities, Beijing and Tianjin, one prefecture-level city was chosen from each of the other four provinces based on the largest growth in urban population from 2001 to 2020. These representative cities are Shijiazhuang, Zhengzhou, Jinan, and Taiyuan. The urban population data were sourced from the annual statistical bulletins of each province. Based on the changes in urban area between 2001 and 2020, the regions of most significant surface change, specifically urban expansion areas (UEA) where the surface transformed from vegetation to urban areas from 2001 to 2020, were identified in each representative city (Fig. 2b). These regions will be the focus of the subsequent discussion.

Results and discussion

Model evaluation

The meteorological parameters selected for evaluating the WRF model performance include 2-m temperature (T2, °C) and 10-m wind speed (W10, m/s). The evaluation period is July 2020, excluding the model spin-up time. From Table S5, it can be observed that the WRF model effectively reproduced the variations in T2 across all study areas, with all regions exhibiting MB values less than 1.0 and ME values less than 2.6. Regarding W10, MB and ME ranged from 0.92 to 1.23 and from 1.72 to 2.31, respectively, indicating a tendency for the model to slightly overestimate in all regions. This may be attributed to regional atmospheric dynamics and model parameterization³¹. Regional atmospheric dynamics may have caused discrepancies between actual conditions and model simulations, and certain simplifications or assumptions in the model parameterization process may have further amplified these differences. The model validation results of this study are consistent with other studies using the WRF model in China^{59–61}. Overall, the simulation of meteorological parameters by WRF for the NCP region is deemed acceptable.

Table S6 presents the performance evaluation results of the CMAQ model using observed O₃ concentrations. The results indicate that NMB values for most regions meet the standards proposed by Emery et al.⁶² (standard values: NMB < ± 15%, NME < ± 25%, R > 0.50). Although a few regions exceed the standards, the maximum NMB value is only –0.22, with all NME values less than 0.45 and R values greater than 0.6. These findings are similar to results from other studies focusing on the NCP region^{6,63}. Overall, the simulation results of the CMAQ model are reliable and can be used for the subsequent content of this study.

Direct impact of LULCC on meteorological parameters

LULCC can regulate the surface energy balance by altering local surface roughness length, radiative albedo, and vegetation stomatal resistance, and it affects the surface material exchange^{64,65}. To study the impact of LULCC on meteorological parameters, we quantified the effects of LULCC on sensible heat flux (SHF), 2-m temperature,

Scenario	Land use and land cover	Meteorology data	Anthropogenic emission
Case 2001	2001	WRF_2020	MEIC_2020
Case 2020	2020	WRF_2020	MEIC_2020

Table 1. Model simulation scenario setting.

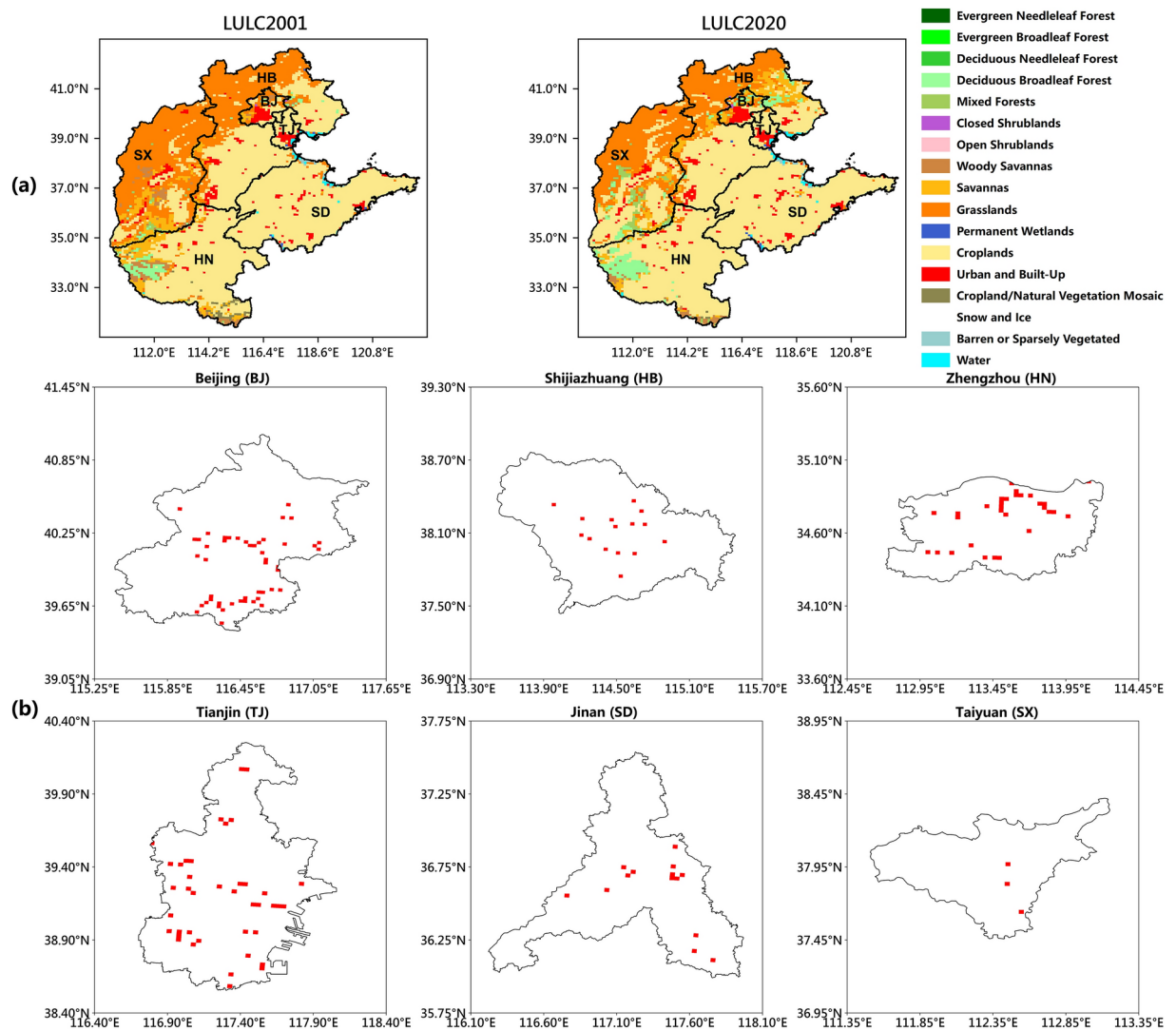


Fig. 2. Comparison of land use and land cover data between 2001 and 2020 (a), and schematic maps depicting the spatial distribution of UEA in the selected six representative cities (b). In (b), the red rectangular grids represent UEA regions, with a grid resolution of 3 km. The parentheses following the city names represent the province or municipality directly under the central government.

10-m wind speed, and planetary boundary layer height (PBLH) in the study area under the two scenarios. For each meteorological parameter, we mapped the spatial distribution of changes induced by LULCC (Figs. 3, 4, 5 and 6). To more clearly study the diurnal and nocturnal differences in the impact of LULCC on meteorological parameters and surface O_3 concentration, this paper defines the period from 08:00 to 19:00 local time as daytime and from 20:00 to 07:00 the next day as nighttime.

As shown in Fig. 3, SHF, being a major component of turbulent exchange between the urban canopy and the atmospheric boundary layer⁶⁶, increased in the UEA regions of the six representative cities both during the daytime and nighttime. The average nighttime increase ranged from 0.12 to 6.94 W/m^2 , while the daytime increase was more significant, with an average growth of 6.49 to 23.46 W/m^2 . From the spatial distribution, it can be seen that the areas of SHF increase highly overlap with the UEA regions. This may be due to the higher heat capacity of artificial materials, causing urban surfaces to absorb more solar radiation and store more heat^{67,68}, leading to a significant increase in sensible heat flux. The increased sensible heat flux raises the surface temperature and enhances vertical turbulence between the surface and the air^{12,69,70}. The changes in T2 are similar to those in SHF, with areas of significant increase also highly overlapping with the UEA regions (Fig. 4). The UEA regions of the six representative cities experienced noticeable temperature increases throughout the entire day. The average daytime increase ranged from 0.14 to 0.31 °C, while the nighttime increase was more pronounced, with an average increase ranging from 0.20 to 0.59 °C. As land use types gradually transition to urban land, urban cement pavements and various artificial materials, which have a strong ability to absorb solar radiation, store a large amount of heat during the daytime. Consequently, these urban areas release the stored heat at night, significantly increasing surface temperatures. The slightly lower daytime temperature increases in UEA regions compared to nighttime may be due to the higher thermal inertia of the urban canopy, which

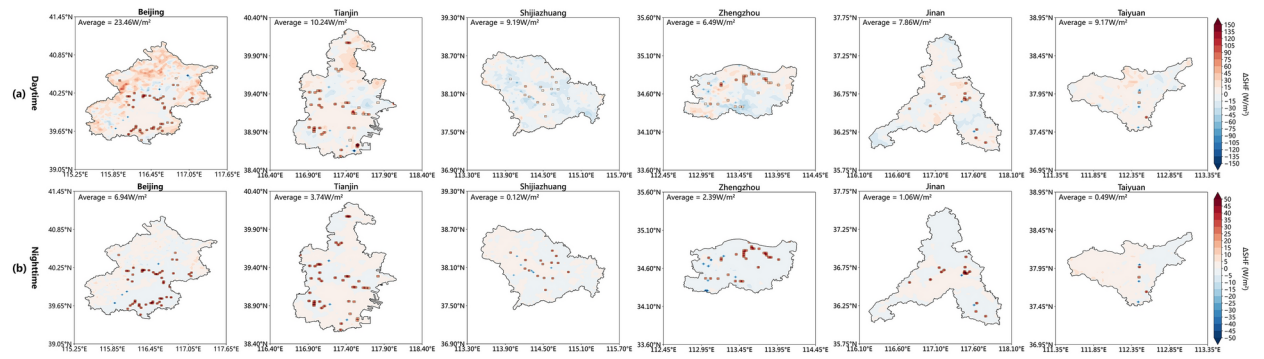


Fig. 3. Spatial distribution of changes in SHF during daytime and nighttime under the influence of LULCC in six representative cities. Daytime refers to 08:00–19:00 local time (a), and nighttime refers to 20:00–07:00 local time the next day (b). The average values in the figure represent the average change in SHF in the UEA regions during these time periods. The gray-bordered grids are used to mark the UEA regions of the representative cities.

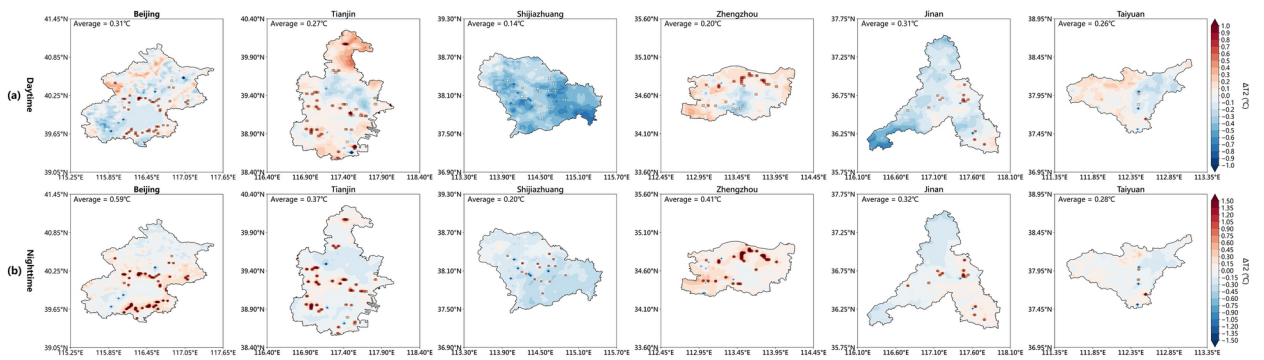


Fig. 4. Spatial distribution of changes in T2 during daytime and nighttime under the influence of LULCC in six representative cities. Daytime refers to 08:00–19:00 local time (a), and nighttime refers to 20:00–07:00 local time the next day (b). The average values in the figure represent the average change in T2 in the UEA regions during these time periods. The gray-bordered grids are used to mark the UEA regions of the representative cities.

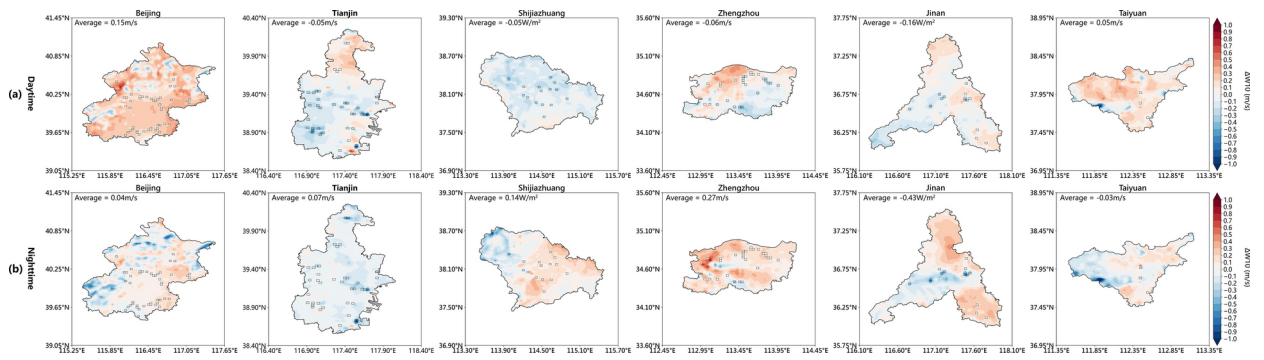


Fig. 5. Spatial distribution of changes in W10 during daytime and nighttime under the influence of LULCC in six representative cities. Daytime refers to 08:00–19:00 local time (a), and nighttime refers to 20:00–07:00 local time the next day (b). The average values in the figure represent the average change in W10 in the UEA regions during these time periods. The gray-bordered grids are used to mark the UEA regions of the representative cities.

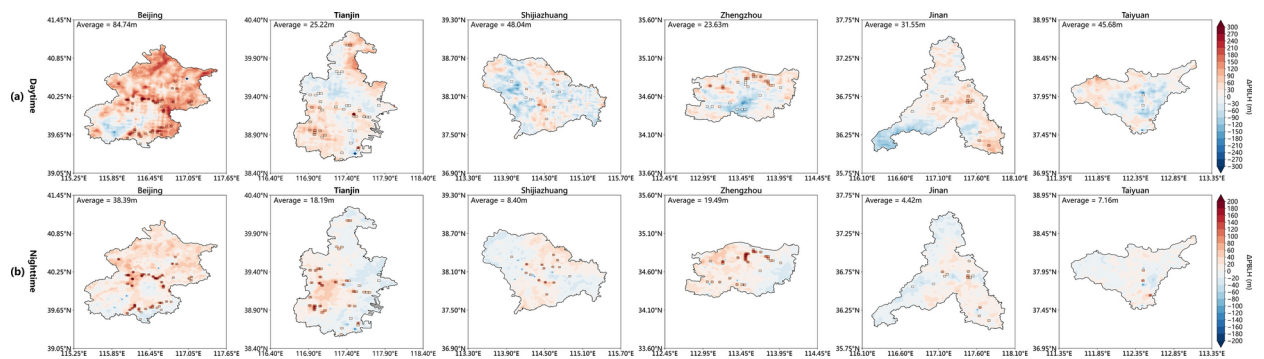


Fig. 6. Spatial distribution of changes in PBLH during daytime and nighttime under the influence of LULCC in six representative cities. Daytime refers to 08:00–19:00 local time (a), and nighttime refers to 20:00–07:00 local time the next day (b). The average values in the figure represent the average change in PBLH in the UEA regions during these time periods. The gray-bordered grids are used to mark the UEA regions of the representative cities.

slows down the warming process during the day^{32,71}. For W10, the UEA regions of the six representative cities generally showed a decreasing trend, but the decrease was relatively slight. In some cities, W10 decreased at night while increasing during the daytime (Fig. 5). The overall range of change was from -0.43 to 0.27 m/s at night and from -0.16 to 0.15 m/s during the day. The increase in nighttime wind speed is mainly attributed to temperature changes (Fig. S1). As nighttime temperatures rise, wind speeds also increase correspondingly. The stronger heat retention capacity of artificial materials leads to a larger temperature difference with the surroundings, and this greater energy differential enhances W10. This is similar to the conclusion reached by Chang et al., who found that urbanization led to an increase in wind speed in southern Taiwan by 0.5 m/s during the day and 1.2 m/s at night⁷². This can be attributed to the heating differences between urban surfaces and surrounding farmland surfaces. For PBLH, the UEA regions of the six representative cities generally exhibited an overall increasing trend throughout the day, with the increase being more pronounced during the daytime (Fig. 6). The average nighttime change ranged from 4.42 to 38.39 m, while the average daytime change ranged from 23.63 to 84.74 m. The changes in PBLH can be attributed to variations in T2 and sensible heat flux. After sunrise, solar radiation heats the surface air, gradually increasing the temperature and enhancing atmospheric turbulence. Considering the higher heat capacity of urban surfaces, vertical mixing intensifies. Additionally, the larger increase in sensible heat flux during the day leads to a more pronounced increase in PBLH during the daytime, while the increase is weaker at night^{73,74}.

Overall, from 2001 to 2020, the UEA regions of the six representative cities show an overall increase in SHF, T2, and PBLH throughout the day, while W10 exhibits a trend of nighttime decrease and daytime increase. The spatial distribution of the changes in meteorological parameters corresponds to the UEA regions, indicating that LULCC leads to these changes in meteorological parameters. This result is consistent with findings from previous studies^{27,31,32}, although there may be variations in the study areas and the magnitudes of changes in meteorological parameters, the overall trend of LULCC's impact on meteorological parameters remains consistent.

1.3. Indirect Impact of LULCC on Surface O_3 and Analysis of Physical and Chemical Pathways.

LULCC can directly affect surface O_3 concentrations by altering surface vegetation cover and land use, thereby impacting natural and anthropogenic emissions. On the other hand, it can indirectly influence surface O_3 concentrations by changing surface albedo and plant transpiration, which in turn affect regional temperature and atmospheric circulation⁷⁵. Previous studies have shown that O_3 concentrations can increase due to the influence of meteorological conditions, external transport, and stratospheric transport^{76–79}. Figure 7 shows the spatial distribution of the monthly average surface O_3 concentration differences for the six representative cities from 2001 to 2020. As can be seen from the figure, the impact of LULCC on surface O_3 is mainly concentrated in the UEA regions, with the areas of significant change highly overlapping with the UEA regions of the six representative cities. In terms of temporal variation, the impact of LULCC resulted in an all-day increase in surface O_3 concentrations in the UEA regions. The average daytime increase ranged from 2.89 to 9.82 $\mu\text{g}/\text{m}^3$, while the average nighttime increase ranged from 1.76 to 7.77 $\mu\text{g}/\text{m}^3$. Therefore, it can be inferred that LULCC enhances the heat storage capacity and increases surface roughness in the UEA regions during the daytime, providing favorable conditions for the production and accumulation of surface O_3 .

To gain a clearer understanding of the indirect impact pathways of LULCC on surface O_3 , we conducted an hourly analysis of the physical and chemical processes affecting surface O_3 formation in the UEA regions. Based on the changes in these processes under the two scenarios, we created Fig. 8. It can be observed that the impact of LULCC on various physical and chemical processes is mainly concentrated during the daytime, while the effects are relatively weaker at night. Under the influence of LULCC, the contribution of the CHEM process gradually increases, promoting surface O_3 formation during the daytime and reducing surface O_3 concentration at night. This may be related to the increased temperature, which enhances various photochemical reactions, including both the formation and removal of surface O_3 ⁸⁰. Apart from the CHEM process, the VTRA process also shows an increase in surface O_3 concentration, indicating that vertical turbulence continuously supplies surface O_3 .

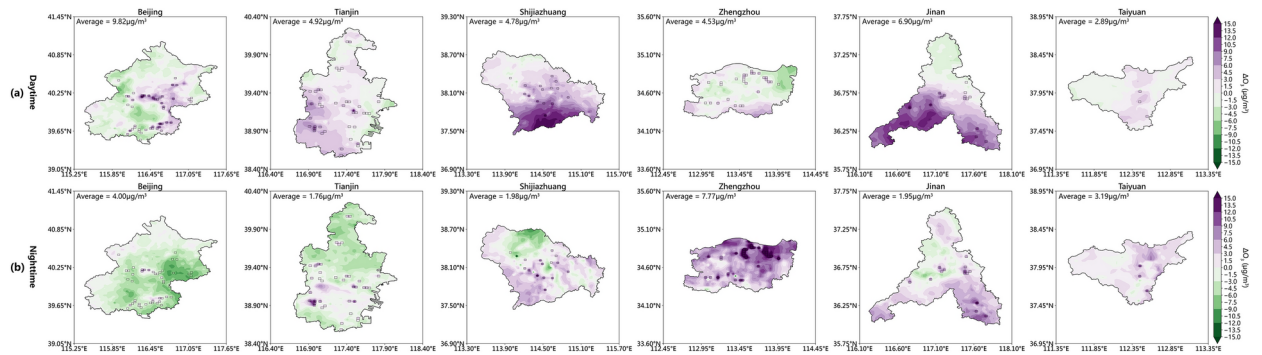


Fig. 7. Spatial distribution of changes in the monthly average surface O_3 concentration during daytime and nighttime under the influence of LULCC in six representative cities. Daytime refers to 08:00–19:00 local time (a), and nighttime refers to 20:00–07:00 local time the next day (b). The average values in the figure represent the average change in O_3 in the UEA regions during these time periods. The gray-bordered grids are used to mark the UEA regions of the representative cities.

from aloft. The enhanced temperature and PBLH promote vertical atmospheric movement within the planetary boundary layer, transporting more O_3 to the surface^{81,82}. However, it was observed that the VTRA process in Beijing promotes O_3 reduction during the daytime. This could be due to the significant urban heat island effect in large cities, where vertical upward airflows above the urban area may transport O_3 away from the surface^{83,84}. The HTRA and DEPO processes predominantly mitigate surface O_3 concentration. The enhanced wind speed during the daytime intensifies the HTRA process's role in reducing surface O_3 , and the DEPO process also contributes more to O_3 reduction due to the influence of LULCC. It was observed that the DEPO process in Beijing increased surface O_3 during the daytime. This may be due to the significant reduction in vegetation in highly developed urban areas, which leads to a diminished role of dry deposition in removing O_3 , thus resulting in a positive contribution to O_3 concentration⁸⁵. The red line in the Fig. 8 represents the overall change in surface O_3 concentration due to LULCC, including both the direct impact through emission inventories and the indirect impact through physical and chemical processes. The blue line represents the combined effect of various physical and chemical processes. It can be seen that the overall trend of indirect impacts remains consistent with the total change, contributing significantly to both the increase and decrease of surface O_3 . This demonstrates that the indirect effects of LULCC on surface O_3 through various physical and chemical processes are significant and cannot be ignored.

When the underlying surface properties change, urban surfaces replace land, and urban buildings replace the original vegetation, which inevitably impacts vertical height as well. Therefore, we created hourly distribution charts of O_3 concentration from the surface to 5000 m for the six representative cities and analyzed the indirect effects of various physical and chemical processes at vertical levels (Fig. 9). After conducting a vertical analysis of O_3 concentration in the UEA regions of the representative cities, we found that the impact of LULCC on O_3 concentration is not limited to the near-surface level. This influence can extend up to the top of the planetary boundary layer (approximately 1500 m), a phenomenon observed in all six representative cities (Fig. S2). Within the space above the surface and below 500 m, the processes that increase and decrease O_3 concentration are the VTRA and HTRA processes, respectively. This is because, near the surface, vertical turbulence and horizontal advection are both enhanced by meteorological factors, making their effects on O_3 enhancement and reduction more significant. Above 500 m, horizontal advection carries O_3 from distant areas, leading to an accumulation of O_3 at certain heights. This accumulated O_3 is then mixed throughout the planetary boundary layer by vertical turbulence⁸⁶, a phenomenon that is intensified by LULCC. Additionally, the CHEM process induced by LULCC promotes O_3 formation not only at the surface but also shows an enhanced effect above the surface. On the other hand, the DEPO process primarily affects surface O_3 concentrations, having a relatively smaller impact on O_3 concentrations above the surface.

Conclusion

In this study, we used the 2020 land use and land cover data obtained from the MODIS satellite to replace the default 2001 data in the WRF-CMAQ model. The modeling study investigated the direct impact of LULCC on meteorological parameters and the indirect impact on surface O_3 concentration through physical and chemical processes in the North China Plain during July in the summer.

To clearly demonstrate the impact of urbanization on meteorological factors and air quality in the North China Plain, we selected six representative cities that have undergone rapid urbanization to represent the overall changes in the region. The study results indicate that LULCC led to significant increases in SHF and T2 throughout the diurnal cycle, particularly during daytime. This may be attributed to the absorption of solar radiation by urban building materials. Regarding W10, most urban areas experienced a decrease in wind speed during nighttime and an increase during daytime. This could be linked to urbanization causing increased surface temperature differentials, which affect wind speeds. Additionally, research on PBLH revealed that UEA regions generally exhibited an increasing trend throughout the diurnal cycle, particularly with more pronounced increases during daytime. This could be attributed to enhanced atmospheric turbulence due to elevated surface

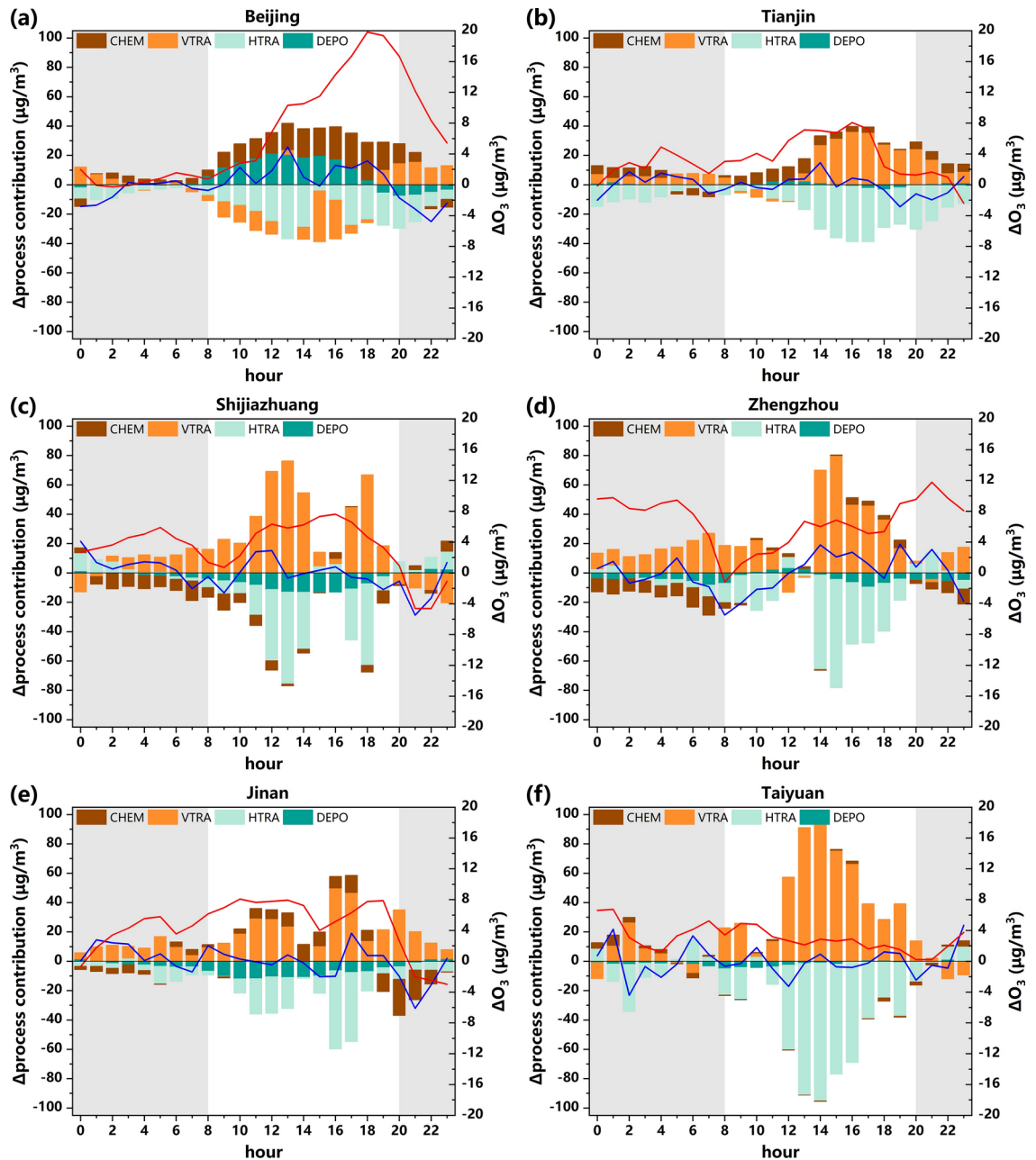


Fig. 8. Hourly contributions of various physical and chemical processes (CHEM: chemical processes, HTRA: horizontal transport, VTRA: vertical transport, DEPO: deposition processes) to surface O_3 concentration in the UEA regions of representative cities (a–f) under the two scenarios. The bar charts represent the contributions of each process, the red line indicates the overall change in surface O_3 concentration due to LULCC, and the blue line represents the combined contributions of all physical and chemical processes due to LULCC, which is the indirect effect of LULCC focused on in this study. Daytime refers to 08:00–19:00 local time (unshaded area), and nighttime refers to 20:00–07:00 local time the next day (shaded area).

temperatures in urban areas. The study found that the O_3 concentration in the UEA regions increased significantly during both daytime and nighttime due to LULCC. The average increase during the daytime ranged from 2.89 to 9.82 $\mu\text{g}/\text{m}^3$, and during the nighttime from 1.76 to 7.77 $\mu\text{g}/\text{m}^3$. The analysis of physical and chemical processes indicates that LULCC enhances meteorological and chemical processes, as well as vertical transport, leading to an increase in O_3 , while horizontal transport and dry deposition processes reduce the O_3 increase. These physical and chemical processes also exhibit diurnal variations. The CHEM process promotes the formation of surface O_3 during the day and reduces surface O_3 concentrations at night. The HTRA and DEPO processes primarily reduce O_3 accumulation during the day, with weaker effects at night. The VTRA process contributes to O_3 accumulation throughout the day. A notable exception is Beijing, where the VTRA process dilutes O_3 and the DEPO process accumulates O_3 . This phenomenon may be related to the urban heat island circulation in

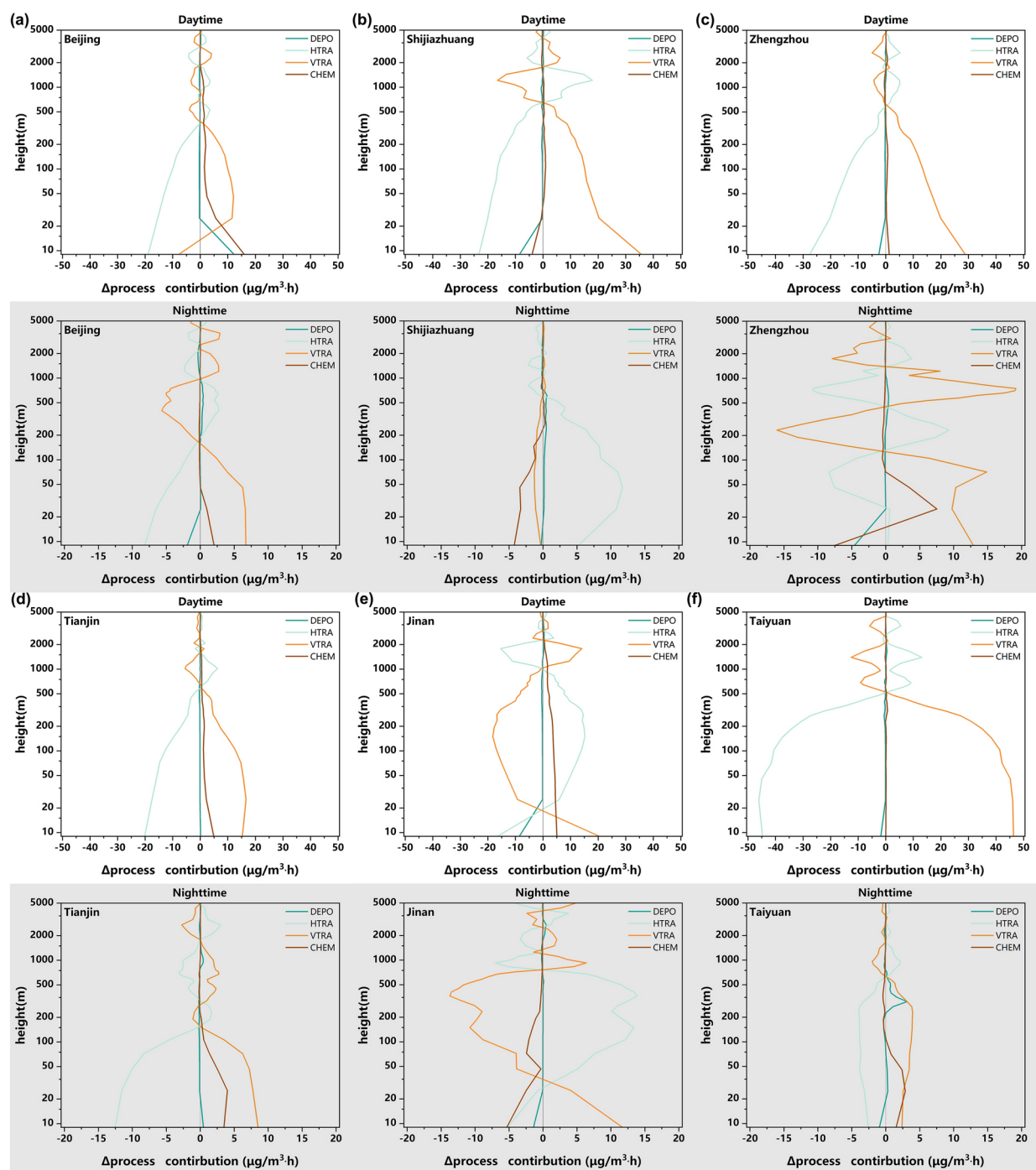


Fig. 9. Vertical distribution of hourly differences in O_3 concentration under the influence of LULCC in the UEA regions of representative cities (a–f), along with the contributions of various physical and chemical processes (CHEM: chemical processes, HTRA: horizontal transport, VTRA: vertical transport, DEPO: deposition processes) to O_3 concentration changes in the vertical direction. The contributions are separated into daytime (with a white background) and nighttime (with a gray background) periods according to local time.

mega-cities and the relatively sparse vegetation. The impact of LULCC on O_3 concentrations is not limited to the surface but extends up to the top of the planetary boundary layer (approximately 1500 m). Below 500 m, vertical transport processes have increased O_3 concentrations while horizontal transport processes have decreased them. Additionally, meteorological and chemical processes influenced by LULCC show enhanced effects above the surface, whereas dry deposition has a minimal impact on ozone concentrations above the ground. Overall, both the direct impacts of LULCC on meteorological parameters and its indirect effects through physical and chemical processes on surface ozone concentrations are significant.

By summarizing previous case studies on air quality modeling, Yang et al.²⁸ proposed that optimizing land use data could improve simulation accuracy. However, previous studies on LULCC have primarily focused on large-scale regions such as the global^{75,87}, Asia^{25,88}, the United States⁸⁹, and China⁹⁰, while smaller-scale studies have concentrated on popular areas such as the Beijing-Tianjin-Hebei region³⁴, the Southwest Basin³¹, and the Yangtze River Delta³³. There has been relatively limited research on the North China Plain. In this study, we took the North China Plain as an example to investigate the impact of urban expansion on meteorological parameters and air quality in the region. This research will contribute to optimizing the simulation accuracy of regional air quality models and help understand the changes in meteorological fields and regional air quality brought about by the rapid development of large cities. It will provide valuable insights for formulating future regional air quality improvement policies and sustainable development goals.

Data availability

Data is provided within the manuscript or supplementary information files.

Received: 16 April 2024; Accepted: 7 January 2025

Published online: 15 January 2025

References

1. Yu, Y. J., Dai, C., Wei, Y. G., Ren, H. M. & Zhou, J. W. Air pollution prevention and control action plan substantially reduced PM_{2.5} concentration in China. *Energy Econ.* **113**, 106206. <https://doi.org/10.1016/j.eneco.2022.106206> (2022).
2. Shu, Y. et al. Analysis of the air pollution reduction and climate change mitigation effects of the Three-Year Action Plan for Blue Skies on the “2+26” Cities in China. *J. Environ. Manag.* **317**, 115455. <https://doi.org/10.1016/j.jenvman.2022.115455> (2022).
3. Qi, L. et al. Collaborative control of fine particles and ozone required in China for health benefit. *Front. Environ. Sci. Eng.* <https://doi.org/10.1007/s11783-023-1692-2> (2023).
4. Kong, S. J., Wang, T., Li, F., Yan, J. J. & Qu, Z. G. Unraveling spatiotemporal patterns and multiple driving factors of surface ozone across China and its urban agglomerations management strategies. *Front. Ecol. Evol.* <https://doi.org/10.3389/fevo.2023.1103503> (2023).
5. Sun, J. et al. Long-term variations of meteorological and precursor influences on ground ozone concentrations in Jinan, north China plain, from 2010 to 2020. *Atmosphere* **13**, 994. <https://doi.org/10.3390/atmos13060994> (2022).
6. Cao, J. Y. et al. Identifying the dominant driver of elevated surface ozone concentration in North China plain during summertime 2012–2017. *Environ. Pollut.* **300**, 118912. <https://doi.org/10.1016/j.envpol.2022.118912> (2022).
7. Yang, L. et al. Ozone exposure and health risks of different age structures in major urban agglomerations in People’s Republic of China from 2013 to 2018. *Environ. Sci. Pollut. Res.* **30**, 42152–42164. <https://doi.org/10.1007/s11356-022-24809-5> (2023).
8. Li, Q. et al. Legacy effects of elevated ozone on soil biota and plant growth. *Soil Biol. Biochem.* **91**, 50–57. <https://doi.org/10.1016/j.soilbio.2015.08.029> (2015).
9. Xu, Y. F. et al. A quantitative assessment and process analysis of the contribution from meteorological conditions in an O₃ pollution episode in Guangzhou, China. *Atmos. Environ.* **303**, 119757. <https://doi.org/10.1016/j.atmosenv.2023.119757> (2023).
10. Li, K. et al. Anthropogenic drivers of 2013–2017 trends in summer surface ozone in China. *Proc. Natl. Acad. Sci. U. S. A.* **116**, 422–427. <https://doi.org/10.1073/pnas.1812168116> (2019).
11. Zhan, C. C. et al. Impacts of urbanization on air quality and the related health risks in a city with complex terrain. *Atmos. Chem. Phys.* **23**, 771–788. <https://doi.org/10.5194/acp-23-771-2023> (2023).
12. Gong, C. et al. Persistent ozone pollution episodes in North China exacerbated by regional transport. *Environ. Pollut.* **265**, 115056. <https://doi.org/10.1016/j.envpol.2020.115056> (2020).
13. Derwent, R. G. et al. Photochemical ozone formation in north west Europe and its control. *Atmos. Environ.* **37**, 1983–1991. [https://doi.org/10.1016/s1352-2310\(03\)00031-1](https://doi.org/10.1016/s1352-2310(03)00031-1) (2003).
14. Xia, Y. et al. Concurrent hot extremes and high ultraviolet radiation in summer over the Yangtze Plain and their possible impact on surface ozone. *Environ. Res. Lett.* **17**, 06400. <https://doi.org/10.1088/1748-9326/ac6c3c> (2022).
15. Tzani, C., Varotsos, C. & Viras, L. Impacts of the solar eclipse of 29 March 2006 on the surface ozone concentration, the solar ultraviolet radiation and the meteorological parameters at Athens, Greece. *Atmos. Chem. Phys.* **8**, 425–430. <https://doi.org/10.5194/acp-8-425-2008> (2008).
16. Belan, B. D. & Savkin, D. E. The role of air humidity in variations in near-surface ozone concentration. *Atmos. Ocean. Opt.* **32**, 586–589. <https://doi.org/10.1134/s1024856019050038> (2019).
17. Newchurch, M. J., Sun, D., Kim, J. H. & Liu, X. Tropical tropospheric ozone derived using Clear-Cloudy Pairs (CCP) of TOMS measurements. *Atmos. Chem. Phys.* **3**, 683–695. <https://doi.org/10.5194/acp-3-683-2003> (2003).
18. Darby, L. S. et al. Vertical variations in O₃ concentrations before and after a gust front passage. *J. Geophys. Res. Atmos.* **107**, 200. <https://doi.org/10.1029/2001jd000996> (2002).
19. Ma, Z. Q., Zhang, X. L., Xu, J., Zhao, X. J. & Meng, W. Characteristics of ozone vertical profile observed in the boundary layer around Beijing in autumn. *J. Environ. Sci.* **23**, 1316–1324. [https://doi.org/10.1016/s1001-0742\(10\)60557-8](https://doi.org/10.1016/s1001-0742(10)60557-8) (2011).
20. Li, K. et al. Ozone pollution in the North China Plain spreading into the late-winter haze season. *Proc. Natl. Acad. Sci. U. S. A.* **118**, 200. <https://doi.org/10.1073/pnas.2015797118> (2021).
21. Fu, D. L. et al. Impacts of maximum snow albedo and land cover changes on meteorological variables during winter in northeast China. *Atmos. Res.* **254**, 105449. <https://doi.org/10.1016/j.atmosres.2021.105449> (2021).
22. Gao, Z. Q., Gao, W. & Slusser, J. In *Conference on Remote Sensing and Modeling of Ecosystems for Sustainability III* (2006).
23. Bagley, J. E., Desai, A. R., West, P. C. & Foley, J. A. A simple, minimal parameter model for predicting the influence of changing land cover on the land-atmosphere system. *Earth Interact.* **15**, 1–32. <https://doi.org/10.1175/2011ei394.1> (2011).
24. Singh, D. et al. Distinct influences of land cover and land management on seasonal climate. *J. Geophys. Res. Atmos.* **123**, 12017–12039. <https://doi.org/10.1029/2018jd028874> (2018).
25. Fu, Y. & Tai, A. P. K. Impact of climate and land cover changes on tropospheric ozone air quality and public health in East Asia between 1980 and 2010. *Atmos. Chem. Phys.* **15**, 10093–10106. <https://doi.org/10.5194/acp-15-10093-2015> (2015).
26. Sharma, S., Chatani, S., Mahtta, R., Goel, A. & Kumar, A. Sensitivity analysis of ground level ozone in India using WRF-CMAQ models. *Atmos. Environ.* **131**, 29–40. <https://doi.org/10.1016/j.atmosenv.2016.01.036> (2016).
27. Qiu, J. X., Fang, C. S., Tian, N. X., Wang, H. F. & Wang, J. Impacts of land use and land cover changes on local meteorology and PM_{2.5} concentrations in Changchun, Northeast China. *Atmos. Res.* **289**, 106759. <https://doi.org/10.1016/j.atmosres.2023.106759> (2023).
28. Yang, J. Y. & Zhao, Y. Performance and application of air quality models on ozone simulation in China—A review. *Atmos. Environ.* **293**, 119446. <https://doi.org/10.1016/j.atmosenv.2022.119446> (2023).
29. Qu, R. J., Cui, X. L., Yan, H. M., Ma, E. J. & Zhan, J. Y. Impacts of land cover change on the near-surface temperature in the north China plain. *Adv. Meteorol.* **2013**, 409302. <https://doi.org/10.1155/2013/409302> (2013).

30. Jiang, X. Y., Wiedinmyer, C., Chen, F., Yang, Z. L. & Lo, J. C. F. Predicted impacts of climate and land use change on surface ozone in the Houston, Texas, area. *J. Geophys. Res. Atmos.* <https://doi.org/10.1029/2008jd009820> (2008).
31. Lu, Y. Q. et al. Exploring the effects of land use and land cover changes on meteorology and air quality over Sichuan Basin, southwestern China. *Front. Ecol. Evol.* **11**, 1131389. <https://doi.org/10.3389/fevo.2023.1131389> (2023).
32. Wang, H. F. et al. Impact of urbanization on meteorology and air quality in Chengdu, a Basin City of Southwestern China. *Front. Ecol. Evol.* **10**, 845801. <https://doi.org/10.3389/fevo.2022.845801> (2022).
33. Li, L. et al. Modeling the impacts of land use/land cover change on meteorology and air quality during 2000–2018 in the Yangtze River Delta region, China. *Sci. Total Environ.* **829**, 154669. <https://doi.org/10.1016/j.scitotenv.2022.154669> (2022).
34. Tao, H. et al. Impacts of land use and land cover change on regional meteorology and air quality over the Beijing–Tianjin–Hebei region, China. *Atmos. Environ.* **189**, 9–21. <https://doi.org/10.1016/j.atmosenv.2018.06.033> (2018).
35. Skamarock, W., Klemp, J., Dudhia, J., Gill, D. O., Liu, Z., Berner, J., Wang, W., Powers, J. G., Duda, M. G., Barker, D. & Huang, X.-Y. A Description of the advanced research WRF model version 4.3. <https://doi.org/10.5065/1dfh-6p97> (2021).
36. Contributor. Research Data Archive at the National Center for Atmospheric Research, Computational and Information Systems Laboratory (2000).
37. Development, U. E. O. o. R. a. CMAQ (5.4). *Zenodo*. 10.5281/zenodo.7218076 (2022).
38. Li, J. et al. Evaluation of the WRF-CMAQ model performances on air quality in China with the impacts of the observation nudging on meteorology. *Aerosol Air Qual. Res.* **22**, 220023. <https://doi.org/10.4209/aaqr.220023> (2022).
39. He, J. J., Yu, Y., Yu, L. J., Liu, N. & Zhao, S. P. Impacts of uncertainty in land surface information on simulated surface temperature and precipitation over China. *Int. J. Climatol.* **37**, 829–847. <https://doi.org/10.1002/joc.5041> (2017).
40. Chen, L. et al. Process-level quantification on opposite PM_{2.5} changes during the COVID-19 lockdown over the north China plain. *Environ. Sci. Technol. Lett.* **10**, 779–785. <https://doi.org/10.1021/acs.estlett.3c00490> (2023).
41. Qiu, J., Fang, C., Tian, N., Wang, H. & Wang, J. Impacts of land use and land cover changes on local meteorology and PM_{2.5} concentrations in Changchun, Northeast China. *Atmos. Res.* **289**, 106759. <https://doi.org/10.1016/j.atmosres.2023.106759> (2023).
42. Tian, J., Wang, J., Wang, D. & Fang, C. Influence of urbanization on meteorological conditions and ozone pollution in the Central Plains Urban Agglomeration, China. *Environ. Pollut.* **356**, 124290. <https://doi.org/10.1016/j.envpol.2024.124290> (2024).
43. Li, M. et al. Anthropogenic emission inventories in China: A review. *Natl. Sci. Rev.* **4**, 834–866. <https://doi.org/10.1093/nsr/nwx150> (2017).
44. Zheng, B. et al. Trends in China's anthropogenic emissions since 2010 as the consequence of clean air actions. *Atmos. Chem. Phys.* **18**, 14095–14111. <https://doi.org/10.5194/acp-18-14095-2018> (2018).
45. Gunther, A. B. et al. The Model of Emissions of Gases and Aerosols from Nature version 2.1 (MEGAN2.1): An extended and updated framework for modeling biogenic emissions. *Geosci. Model Dev.* **5**, 1471–1492 (2012).
46. Esri. ArcGIS Desktop: ArcMap in ArcGIS 10.8 (Environmental systems Research Institute, 2020).
47. Friedl, M. & Sulla-Menashe, D. MODIS/Terra + Aqua land cover type yearly L3 global 500 m SIN Grid V061 (NASA EOSDIS Land Processes Distributed Active Archive Center, 2022). <https://doi.org/10.5067/MODIS/MCD12Q1.061>.
48. Hogrefe, C. et al. Simulating changes in regional air pollution over the eastern United States due to changes in global and regional climate and emissions. *J. Geophys. Res. Atmos.* <https://doi.org/10.1029/2004JD004690> (2004).
49. Jiménez, P., Parra, R. & Baldasano, J. M. Influence of initial and boundary conditions for ozone modeling in very complex terrains: A case study in the northeastern Iberian Peninsula. *Environ. Model. Softw.* **22**, 1294–1306. <https://doi.org/10.1016/j.envsoft.2006.08.004> (2007).
50. Carey Jang, J.-C., Jeffries, H. E., Byun, D. & Pleim, J. E. Sensitivity of ozone to model grid resolution—I. Application of high-resolution regional acid deposition model. *Atmos. Environ.* **29**, 3085–3100. [https://doi.org/10.1016/1352-2310\(95\)00118-1](https://doi.org/10.1016/1352-2310(95)00118-1) (1995).
51. Jang, J.-C.C., Jeffries, H. E. & Tonnesen, S. Sensitivity of ozone to model grid resolution—II. Detailed process analysis for ozone chemistry. *Atmos. Environ.* **29**, 3101–3114. [https://doi.org/10.1016/1352-2310\(95\)00119-1](https://doi.org/10.1016/1352-2310(95)00119-1) (1995).
52. Godowitch, J. M., Gilliam, R. C. & Rao, S. T. Diagnostic evaluation of ozone production and horizontal transport in a regional photochemical air quality modeling system. *Atmos. Environ.* **45**, 3977–3987. <https://doi.org/10.1016/j.atmosenv.2011.04.062> (2011).
53. Ji, D. S. et al. Investigating the evolution of summertime secondary atmospheric pollutants in urban Beijing. *Sci. Total Environ.* **572**, 289–300. <https://doi.org/10.1016/j.scitotenv.2016.07.153> (2016).
54. Clifton, O. E. et al. Influence of dynamic ozone dry deposition on ozone pollution. *J. Geophys. Res. Atmos.* **125**, e2020JD032398. <https://doi.org/10.1029/2020jd032398> (2020).
55. Fu, X. et al. The impacts of ship emissions on ozone in eastern China. *Sci. Total Environ.* **903**, 166252 (2023).
56. Zhu, Y. Q. et al. Assessment of tropospheric ozone simulations in a regional chemical transport model using GEOS-Chem outputs as chemical boundary conditions. *Sci. Total Environ.* **906**, 167485. <https://doi.org/10.1016/j.scitotenv.2023.167485> (2024).
57. Wang, H. L. et al. Seasonality and reduced nitric oxide titration dominated ozone increase during COVID-19 lockdown in eastern China. *Npj Clim. Atmos. Sci.* **5**, 24. <https://doi.org/10.1038/s41612-022-00249-3> (2022).
58. Fu, X. Y. et al. The impacts of ship emissions on ozone in eastern China. *Sci. Total Environ.* **903**, 166252. <https://doi.org/10.1016/j.scitotenv.2023.166252> (2023).
59. Hu, J. L., Chen, J. J., Ying, Q. & Zhang, H. L. One-year simulation of ozone and particulate matter in China using WRF/CMAQ modeling system. *Atmos. Chem. Phys.* **16**, 10333–10350. <https://doi.org/10.5194/acp-16-10333-2016> (2016).
60. Chang, X., Wang, S. X., Zhao, B., Cai, S. Y. & Hao, J. M. Assessment of inter-city transport of particulate matter in the Beijing–Tianjin–Hebei region. *Atmos. Chem. Phys.* **18**, 4843–4858. <https://doi.org/10.5194/acp-18-4843-2018> (2018).
61. Ma, J. L. et al. Modeled changes in source contributions of particulate matter during the COVID-19 pandemic in the Yangtze River Delta, China. *Atmos. Chem. Phys.* **21**, 7343–7355. <https://doi.org/10.5194/acp-21-7343-2021> (2021).
62. Emery, C. et al. Recommendations on statistics and benchmarks to assess photochemical model performance. *J. Air Waste Manag. Assoc.* **67**, 582–598. <https://doi.org/10.1080/10962247.2016.1265027> (2017).
63. Li, J. L. et al. Model analyses of changes in spring surface ozone concentrations over Shandong Province in the period of 2014–2017. *Aerosol Air Qual. Res.* **22**, 220139. <https://doi.org/10.4209/aaqr.220139> (2022).
64. Patel, P., Karmakar, S., Ghosh, S. & Niyogi, D. Improved simulation of very heavy rainfall events by incorporating WUDAPT urban land use/land cover in WRF. *Urban Clim.* **32**, 100616. <https://doi.org/10.1016/j.uclim.2020.100616> (2020).
65. Mahmood, R. et al. Land cover changes and their biogeophysical effects on climate. *Int. J. Climatol.* **34**, 929–953. <https://doi.org/10.1002/joc.3736> (2014).
66. Yang, J. X. et al. Parameterization of urban sensible heat flux from remotely sensed surface temperature: Effects of surface structure. *Remote Sens.* **11**, 1347. <https://doi.org/10.3390/rs11111347> (2019).
67. Gapski, N. H., Marinoski, D. L., Melo, A. P. & Guths, S. Impact of urban surfaces' solar reflectance on air temperature and radiation flux. *Sustain. Cities Soc.* **96**, 104645. <https://doi.org/10.1016/j.scs.2023.104645> (2023).
68. Ziaemehr, B., Jandaghian, Z., Ge, H., Lacasse, M. & Moore, T. Increasing solar reflectivity of building envelope materials to mitigate urban heat islands: State-of-the-art review. *Buildings* **13**, 2868. <https://doi.org/10.3390/buildings13112868> (2023).
69. Brandi, A., Broadbent, A. M., Krayenhoff, E. S. & Georgescu, M. Influence of projected climate change, urban development and heat adaptation strategies on end of twenty-first century urban boundary layers across the Conterminous US. *Clim. Dyn.* **57**, 757–773. <https://doi.org/10.1007/s00382-021-05740-w> (2021).

70. Dupont, E., Menut, L., Carissimo, B., Pelon, J. & Flamant, P. Comparison between the atmospheric boundary layer in Paris and its rural suburbs during the ECLAP experiment. *Atmos. Environ.* **33**, 979–994. [https://doi.org/10.1016/s1352-2310\(98\)00216-7](https://doi.org/10.1016/s1352-2310(98)00216-7) (1999).
71. Qin, Y. H. A review on the development of cool pavements to mitigate urban heat island effect. *Renew. Sustain. Energy Rev.* **52**, 445–459. <https://doi.org/10.1016/j.rser.2015.07.177> (2015).
72. Chang, J. H. W., Griffith, S. M. & Lin, N. H. Impacts of land-surface forcing on local meteorology and ozone concentrations in a heavily industrialized coastal urban area. *Urban Clim.* **45**, 101257. <https://doi.org/10.1016/j.uclim.2022.101257> (2022).
73. Huszar, P., Karlicky, J., Belda, M., Halenka, T. & Pisoft, P. The impact of urban canopy meteorological forcing on summer photochemistry. *Atmos. Environ.* **176**, 209–228. <https://doi.org/10.1016/j.atmosenv.2017.12.037> (2018).
74. Yang, B., Zhang, Y. C. & Qian, Y. Simulation of urban climate with high-resolution WRF model: A case study in Nanjing, China. *Asia Pac. J. Atmos. Sci.* **48**, 227–241. <https://doi.org/10.1007/s13143-012-0023-5> (2012).
75. Wang, L. et al. Impacts of future land use and land cover change on mid-21st-century surface ozone air quality: Distinguishing between the biogeophysical and biogeochemical effects. *Atmos. Chem. Phys.* **20**, 11349–11369. <https://doi.org/10.5194/acp-20-11349-2020> (2020).
76. Hu, C. Y. et al. Understanding the impact of meteorology on ozone in 334 cities of China. *Atmos. Environ.* **248**, 118221. <https://doi.org/10.1016/j.atmosenv.2021.118221> (2021).
77. Lei, Y. et al. Role of meteorology-driven regional transport on O₃ pollution over the Chengdu Plain, southwestern China. *Atmos. Res.* **285**, 106619. <https://doi.org/10.1016/j.atmosres.2023.106619> (2023).
78. Hu, F. et al. Integrated analysis of the transport process and source attribution of an extreme ozone pollution event in Hefei at different vertical heights: A case of study. *Sci. Total Environ.* **906**, 167237. <https://doi.org/10.1016/j.scitotenv.2023.167237> (2024).
79. Ding, J. et al. Impacts of meteorology and precursor emission change on O₃ variation in Tianjin, China from 2015 to 2021. *J. Environ. Sci.* **126**, 506–516. <https://doi.org/10.1016/j.jes.2022.03.010> (2023).
80. Romer, P. S. et al. Effects of temperature-dependent NO_x emissions on continental ozone production. *Atmos. Chem. Phys.* **18**, 2601–2614. <https://doi.org/10.5194/acp-18-2601-2018> (2018).
81. Su, T., Li, Z. & Kahn, R. Relationships between the planetary boundary layer height and surface pollutants derived from lidar observations over China: Regional pattern and influencing factors. *Atmos. Chem. Phys.* **18**, 15921–15935 (2018).
82. Gu, M., Moore, G., Wood, K. & Wang, Z. J. A. Planetary boundary layer heights from cruises in spring to autumn Chukchi-Beaufort Sea compared with ERA5. *Atmosphere* **12**, 1398 (2021).
83. Fallmann, J., Forkel, R. & Emeis, S. Secondary effects of urban heat island mitigation measures on air quality. *Atmos. Environ.* **125**, 199–211. <https://doi.org/10.1016/j.atmosenv.2015.10.094> (2016).
84. Hang, J. & Li, Y. Age of air and air exchange efficiency in high-rise urban areas and its link to pollutant dilution. *Atmos. Environ.* **45**, 5572–5585. <https://doi.org/10.1016/j.atmosenv.2011.04.051> (2011).
85. Cao, J., Pan, G., Zheng, B., Liu, Y. & Zhang, G. Significant land cover change in China during 2001–2019: Implications for direct and indirect effects on surface ozone concentration. *Environ. Pollut.* **335**, 122290 (2023).
86. Yang, H. et al. Effects of horizontal transport and vertical mixing on nocturnal ozone pollution in the Pearl River Delta. *Atmosphere* **13**, 1318 (2022).
87. Wu, S., Mickley, L. J., Kaplan, J. O. & Jacob, D. J. Impacts of changes in land use and land cover on atmospheric chemistry and air quality over the 21st century. *Atmos. Chem. Phys.* **12**, 1597–1609. <https://doi.org/10.5194/acp-12-1597-2012> (2012).
88. Vadrevu, K., Ohara, T. & Justice, C. Land cover, land use changes and air pollution in Asia: A synthesis. *Environ. Res. Lett.* **12**, 120201. <https://doi.org/10.1088/1748-9326/aa9c5d> (2017).
89. Chen, J. et al. Future land use and land cover influences on regional biogenic emissions and air quality in the United States. *Atmos. Environ.* **43**, 5771–5780. <https://doi.org/10.1016/j.atmosenv.2009.08.015> (2009).
90. Cao, Y. et al. Impacts of land cover changes on summer surface ozone in China during 2000–2019. *Sci. Total Environ.* **948**, 174821. <https://doi.org/10.1016/j.scitotenv.2024.174821> (2024).

Acknowledgements

The authors wish to thank all members of the 142 and the 537 research labs.

Author contributions

J.W.: Conceptualization, Writing—Review & Editing, Supervision. X.L.: Conceptualization, Methodology, Formal analysis, Investigation, Data Curation, Writing—Original Draft, Visualization. J.L.: Methodology, Formal analysis, Data Curation, Visualization. J.T.: Methodology, Visualization, Supervision. C.F.: Data Curation, Writing—Review & Editing, Supervision. All authors contributed to the manuscript and approved the submission.

Funding

Supported by Graduate Innovation Fund of Jilin University.

Declarations

Competing interests

The authors declare no competing interests.

Additional information

Supplementary Information The online version contains supplementary material available at <https://doi.org/10.1038/s41598-025-85940-0>.

Correspondence and requests for materials should be addressed to J.W.

Reprints and permissions information is available at www.nature.com/reprints.

Publisher's note Springer Nature remains neutral with regard to jurisdictional claims in published maps and institutional affiliations.

Open Access This article is licensed under a Creative Commons Attribution-NonCommercial-NoDerivatives 4.0 International License, which permits any non-commercial use, sharing, distribution and reproduction in any medium or format, as long as you give appropriate credit to the original author(s) and the source, provide a link to the Creative Commons licence, and indicate if you modified the licensed material. You do not have permission under this licence to share adapted material derived from this article or parts of it. The images or other third party material in this article are included in the article's Creative Commons licence, unless indicated otherwise in a credit line to the material. If material is not included in the article's Creative Commons licence and your intended use is not permitted by statutory regulation or exceeds the permitted use, you will need to obtain permission directly from the copyright holder. To view a copy of this licence, visit <http://creativecommons.org/licenses/by-nc-nd/4.0/>.

© The Author(s) 2025